

## Exciton Binding Energy and Nonhydrogenic Rydberg Series in Monolayer WS<sub>2</sub>

Alexey Chernikov,<sup>1,\*</sup> Timothy C. Berkelbach,<sup>2</sup> Heather M. Hill,<sup>1</sup> Albert Rigosi,<sup>1</sup> Yilei Li,<sup>1</sup> Ozgur Burak Aslan,<sup>1</sup>  
David R. Reichman,<sup>2</sup> Mark S. Hybertsen,<sup>3</sup> and Tony F. Heinz<sup>1,†</sup>

<sup>1</sup>*Departments of Physics and Electrical Engineering, Columbia University, 538 West 120th Street, New York, New York 10027, USA*

<sup>2</sup>*Department of Chemistry, Columbia University, 3000 Broadway, New York, New York 10027, USA*

<sup>3</sup>*Center for Functional Nanomaterials, Brookhaven National Laboratory, Upton, New York 11973-5000, USA*

(Received 12 March 2014; published 13 August 2014)

We have experimentally determined the energies of the ground and first four excited excitonic states of the fundamental optical transition in monolayer WS<sub>2</sub>, a model system for the growing class of atomically thin two-dimensional semiconductor crystals. From the spectra, we establish a large exciton binding energy of 0.32 eV and a pronounced deviation from the usual hydrogenic Rydberg series of energy levels of the excitonic states. We explain both of these results using a microscopic theory in which the nonlocal nature of the effective dielectric screening modifies the functional form of the Coulomb interaction. These strong but unconventional electron-hole interactions are expected to be ubiquitous in atomically thin materials.

DOI: 10.1103/PhysRevLett.113.076802

PACS numbers: 73.20.Mf, 71.35.-y, 73.21.-b, 73.22.-f

Atomically thin materials such as graphene and transition-metal dichalcogenides (TMDs) exhibit remarkable physical properties resulting from their reduced dimensionality [1]. The family of TMDs is an especially promising platform for fundamental studies of two-dimensional (2D) systems, with potential applications in optoelectronics and valleytronics due to their direct gap, semiconducting nature in the monolayer limit [2–7]. The recent advances in this emerging field include strongly enhanced photoluminescence [2,4], efficient spin-valley coupling [8–11], pronounced many-body effects [6,12], and high performance in field-effect transistors [13].

The 2D character of monolayer TMDs suggests a strong enhancement of the Coulomb interaction. The resulting formation of bound electron-hole pairs, or excitons, can dominate the optical and charge-transport properties [14]. A microscopic understanding of how excitons are formed from otherwise free carriers is critical both for the elucidation of the underlying many-body physics in such materials and for their use in electronic and photonic devices. While theoretical and computational studies have predicted exciton binding energies as high as 1 eV [15–19], a direct measurement of the exciton binding energy is still lacking (however, see Noted added).

In this work, we experimentally and theoretically investigate the properties of excitons in mono- and few-layer TMDs, identifying and characterizing not only the ground-state exciton but the full sequence of excited (Rydberg) exciton states. Analyzing our sensitive measurements of the optical reflection spectra of these materials, both empirically and using a physically motivated model for the nonlocal screening in TMDs, results in an estimate of  $0.32(\pm 0.04)$  eV for the  $1s$  exciton binding energy and  $2.41(\pm 0.04)$  eV for the quasiparticle gap of monolayer WS<sub>2</sub>. Remarkably, we also find significant deviations from the conventional hydrogenic model typically employed for the description of

Wannier excitons in inorganic semiconductors [20] and explain our findings in terms of a microscopic theory that highlights the peculiar form taken by the electron-hole interaction in this class of novel materials [21–23].

The specific material studied here is WS<sub>2</sub>, a representative member of the TMD family that includes MoS<sub>2</sub>, MoSe<sub>2</sub>, and WSe<sub>2</sub>, all of which share similar properties with respect to atomic and electronic structure. The advantage of WS<sub>2</sub> for this study is the large spin-orbit splitting between the  $A$  and  $B$  excitons of about 0.4 eV [7], allowing for a study of the low-energy excitons unobscured by features from higher-lying transitions. In addition, the electronic transitions in the WS<sub>2</sub> samples exhibit narrow spectral features, permitting identification and analysis of many excited excitonic states and detailed quantitative comparison with theoretical predictions. Sample preparation and characterization details can be found in the Supplemental Material [24].

Experimental and theoretical studies to date have clearly demonstrated that the basic excitonic properties of a three-dimensional bulk semiconductor differ fundamentally from those of a 2D monolayer of the same material. The real-space origin of this behavior in TMDs is illustrated schematically in Fig. 1(a). In contrast to bulk, the electron and hole forming an exciton in monolayer TMDs are strongly confined to the plane of the monolayer and additionally experience reduced screening due to the change in the dielectric environment. These effects have two major implications for the electronic and excitonic properties of the material, shown by a schematic representation of the optical absorption in Fig. 1(b). First, the quasiparticle band gap is expected to increase for the monolayer. Second, the enhanced electron-hole interaction is expected to increase the exciton binding energy. In the absence of dielectric effects, this yields an exciton binding energy that is a factor of 4 larger in 2D than in 3D. In the limit of atomically thin materials, however, the dielectric screening is also reduced because the electric field

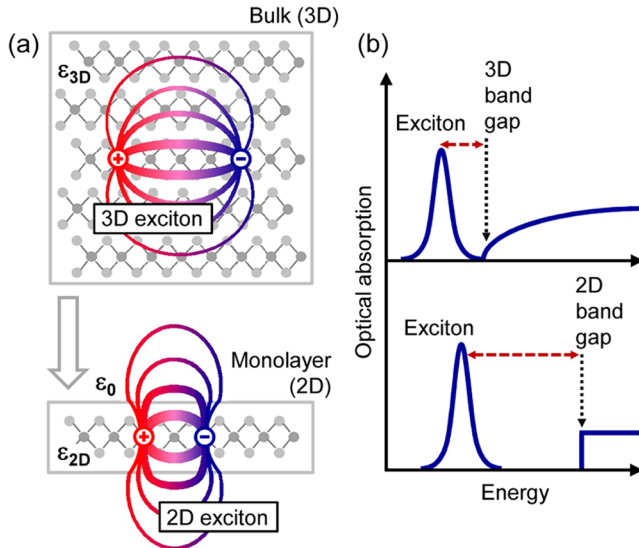


FIG. 1 (color online). (a) Real-space representation of electrons and holes bound into excitons for the three-dimensional bulk and a quasi-two-dimensional monolayer. The changes in the dielectric environment are indicated schematically by different dielectric constants  $\epsilon_{3D}$  and  $\epsilon_{2D}$  and by the vacuum permittivity  $\epsilon_0$ . (b) Impact of the dimensionality on the electronic and excitonic properties, schematically represented by optical absorption. The transition from 3D to 2D is expected to lead to an increase of both the band gap and the exciton binding energy (indicated by the dashed red line). The excited excitonic states and Coulomb correction for the continuum absorption have been omitted for clarity.

lines joining the electron and hole begin to extend outside of the sample, as shown in Fig. 1(a), potentially yielding an even greater enhancement factor. This so-called “dielectric confinement” or “image charge effect” [21,38] was observed in nanostructured materials such as single-walled carbon nanotubes [39] and layered organic-inorganic perovskites [40]. The effectiveness of the dielectric screening thus depends on the separation between the electron and hole. This modifies the form of the interaction potential [21–23,38] and causes a significant change of the disposition of the energies of the excitonic states, as discussed in more detail below.

To access these exciton properties experimentally, we study the so-called excitonic Rydberg series, i.e., the excited states of the bound electron-hole pairs, labeled in analogy to the hydrogen series as  $2s$ ,  $3s$ , and so on. In contrast to  $p$ - or  $d$ -like states with nonzero orbital angular momentum, these transitions are predicted to be dipole allowed [18,19] and are thus observable in the linear optical spectra of TMDs, as well as in most other semiconductors, with peak positions located between the quasiparticle band gap and the exciton  $1s$  ground state [14,20]. The energy separation of these resonances corresponds to a hydrogenic progression for Wannier-like excitons. In addition, the coupling of the excited states to light is reduced compared to the main transition, so that their spectral weight decreases with increasing quantum number.

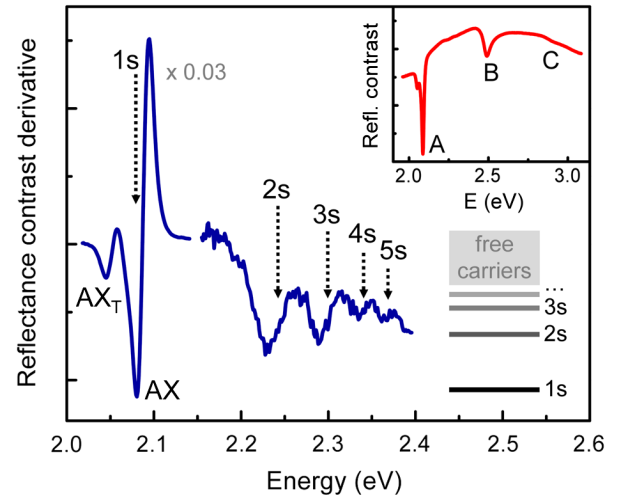


FIG. 2 (color online). The derivative of the reflectance contrast spectrum  $(d/dE)(\Delta R/R)$  of the  $\text{WS}_2$  monolayer. The exciton ground state and the higher excited states are labeled by their respective quantum numbers (schematically shown at the bottom right). The spectral region around the  $1s$  transition ( $AX$ ) and the trion peak ( $AX_T$ ) of the  $A$  exciton is scaled by a factor of 0.03 for clarity. The inset shows the as-measured reflectance contrast  $\Delta R/R$  for comparison, allowing for the identification of the  $A$ ,  $B$ , and  $C$  transitions.

In our experiments, we measure the reflectance contrast  $\Delta R/R = (R_{\text{sample}} - R_{\text{substrate}})/R_{\text{substrate}}$  of the  $\text{WS}_2$  monolayer sample at a temperature of 5 K. The experimental details are given in the Supplemental Material [24]. The spectrum, plotted in the inset of Fig. 2, exhibits several pronounced peaks on a broad background, the latter arising from interference effects induced by the 300 nm thick  $\text{SiO}_2$  layer between the sample and the Si substrate [6]. The main transitions correspond to the so-called  $A$ ,  $B$ , and  $C$  excitons in  $\text{WS}_2$  [7]. A small additional feature on the low-energy side of the  $A$  peak is identified as a charged exciton (or trion), with a binding energy on the order of 20–30 meV. Such a feature has been observed in monolayers of other TMDs at low temperatures [6,12] and indicates the presence of some unintentional residual doping in the  $\text{WS}_2$  sample. Here, we focus on the properties of the  $A$  exciton, related to the fundamental band gap of the material. In order to highlight the otherwise weak signatures of the higher-lying excitonic transitions, we plot in Fig. 2 the derivative of the reflectance contrast  $(d/dE)(\Delta R/R)$  in the energy range of interest. On the high-energy side of the exciton  $1s$  ground state, we observe multiple additional peaks, which we identify as the  $2s$ ,  $3s$ ,  $4s$ , and  $5s$  states of the  $A$  exciton, since the decrease of both the peak intensity and the energy spacing for increasing energy are characteristic features of an excitonic Rydberg series [14,20]. The peak positions extracted by taking the respective points of inflection are plotted in Fig. 3(a). The respective energies are further confirmed by simulating the material response with a multiple-Lorentzian fit (see the Supplemental Material [24]).

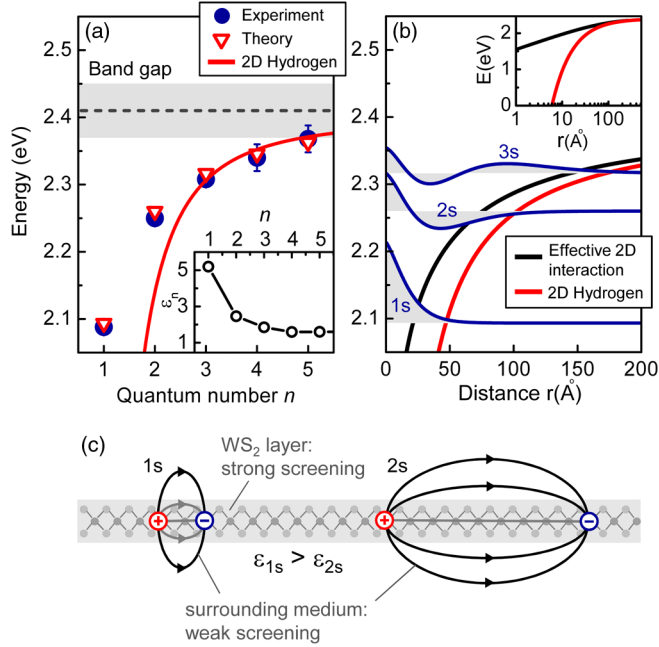


FIG. 3 (color online). (a) Experimentally and theoretically obtained transition energies for the exciton states as a function of the quantum number  $n$ . The fit of the  $n = 3, 4, 5$  data to the 2D hydrogen model for Wannier excitons is shown for comparison. Gray bands represent uncertainty in the quasiparticle band gap from the fitting procedure. Corresponding effective dielectric constants are shown in the inset. (b) Screened 2D interaction Eq. (2) used in the model Hamiltonian (black lines) compared to the 2D hydrogen interaction  $1/r$  (red lines); a semilogarithmic plot is given in the inset. Also shown are the corresponding energy levels and radial wave functions up to  $n = 3$ . (c) Schematic representation of electron-hole pairs forming  $1s$  and  $2s$  excitonic states in a nonuniform dielectric environment.

To calculate the exciton binding energy, we must first determine the quasiparticle band gap corresponding to the energy of a separated electron-hole pair. This is typically accomplished in semiconductors by fitting the excitonic peaks to a hydrogenic Rydberg series [20]. In 2D, this hydrogen model employs an effective mass Hamiltonian  $H = -\hbar^2 \nabla_r^2 / 2\mu + V_{eh}(r)$ , where  $\mu = 1/(m_e^{-1} + m_h^{-1})$  is the exciton reduced mass and  $V_{eh}(r) = -e^2/\epsilon r$  is a locally screened attractive electron-hole interaction. This model predicts exciton transition energies of  $E_g - E_b^{(n)}$ , where  $E_g$  is the quasiparticle gap and

$$E_b^{(n)} = \frac{\mu e^4}{2\hbar^2 \epsilon^2 (n - 1/2)^2} \quad (1)$$

is the binding energy of the  $n$ th excitonic state. In contrast, the exciton energies seen in our experiments exhibit a much weaker scaling with the quantum number  $n$ , precluding a simple fit to the data based on this model. However, we observe that the  $n = 3-5$  peaks are reasonably hydrogenic, and by fitting to these data points only, we extract a quasiparticle band gap of  $E_g = 2.41(\pm 0.04)$  eV, where the

error bars originate from the fitting procedure. Subtracting the  $1s$  transition energy of 2.09 eV from this band gap, we find an exciton binding energy of  $E_b = 0.32(\pm 0.04)$  eV.

To provide insight into the nonhydrogenic physics of the  $n = 1, 2$  excitons and justify a hydrogenic fit to the  $n = 3-5$  excitons, we first consider the use of an effective dielectric constant in the hydrogenic Hamiltonian. Using an exciton reduced mass of  $\mu = 0.16m_0$  (as determined by density functional theory at the  $K$  or  $K'$  point [23,41]; see the Supplemental Material [24]) and the quasiparticle band gap of  $E_g = 2.41$  eV, we determine the  $n$ -dependent dielectric constant  $\epsilon_n$  required to reproduce the experimental binding energy of the  $n$ th exciton  $E_{b,\text{expt}}^{(n)}$ , i.e.,  $\epsilon_n = [2\hbar^2 E_{b,\text{expt}}^{(n)} (n - 1/2)^2 / \mu e^4]^{-1/2}$ . The results plotted in the inset of Fig. 3(a) show a strong decrease in this effective dielectric constant with increasing quantum number  $n$ . Because the exciton radius increases with  $n$ , we conclude that the physically correct electron-hole interaction is more strongly screened at short range but only weakly screened at long range. In particular, the effective dielectric is nearly constant for  $n = 3-5$  (justifying our empirical use of the 2D hydrogen model for these data points) but shows significant deviations for  $n = 1, 2$ . This can be understood qualitatively in terms of a nonuniform dielectric environment schematically illustrated in Fig. 3(c). The electric field between an electron and a hole forming an exciton permeates both the thin layer of material with comparably strong screening and the surrounding medium with much weaker screening. As the spatial separation between the charges increases, a larger portion of the electric field is located in the surrounding low-dielectric medium and the effective screening is reduced. This phenomenon of “antiscreeing,” giving rise to nonhydrogenic exciton behavior, has previously been predicted in carbon nanotubes, a quasi-one-dimensional semiconductor [39].

To understand this behavior quantitatively, we apply our recently developed theory of excitons in transition-metal dichalcogenides [23]. The treatment is again based on a 2D effective mass Hamiltonian but with a nonlocally screened electron-hole interaction described by the potential

$$V_{eh}(r) = -\frac{\pi e^2}{2r_0} \left[ H_0\left(\frac{r}{r_0}\right) - Y_0\left(\frac{r}{r_0}\right) \right], \quad (2)$$

where  $H_0$  and  $Y_0$  are Struve and Bessel functions. This interaction form describes the electrostatic interaction of two charges within a thin 2D dielectric continuum [21,22,38]. The screening length  $r_0$ , which can be related to the 2D polarizability of the monolayer material [22], gives a crossover length scale between a  $1/r$  Coulomb interaction at large separation and a weaker  $\log(r)$  interaction at small separation. This modified functional form of the interaction, which is a manifestation of the strong dielectric contrast between the monolayer  $\text{WS}_2$  and its surroundings, is responsible for the altered disposition of the low-lying excitonic states observed experimentally.

Using the above functional form for the screened interaction, we have numerically calculated the radially symmetric,  $s$ -type eigenstates of the excitonic Hamiltonian, again using the calculated exciton reduced mass  $\mu = 0.16m_0$ . Taking only the screening length  $r_0$  and the band gap  $E_g$  as free parameters, we find that we can very accurately fit the entire  $n = 1-5$  series of exciton levels with the values  $r_0 = 75 \text{ \AA}$  and  $E_g = 2.41 \text{ eV}$ . These are the parameters which minimize the root-mean-squared deviation between theory and experiment. For this choice of parameters, the  $1s$  exciton binding energy is found to be  $0.32 \text{ eV}$ , and so both the band gap and the binding energy are found to agree with the values determined above. We emphasize that the adopted screening length should be understood as one that partially accounts for additional screening due to the substrate, such that the intrinsic binding energy of  $\text{WS}_2$  is expected to be larger than the value found here, in qualitative agreement with *ab initio* calculations [15–17] (see the Supplemental Material for a discussion of the microscopic origin of the precise value of  $r_0$  [24]). Figure 3(b) depicts the noticeably weakened interaction at small electron-hole separations, along with the first three calculated radial wave functions. The spatial extent of the exciton wave function is calculated to be approximately  $30 \text{ \AA}$  for the  $1s$  exciton and even larger for the higher-lying excitons, which supports a strictly 2D treatment when compared to the monolayer width of about  $6 \text{ \AA}$ . Similarly, this relatively large in-plane spatial extent implies a narrow reciprocal space distribution, justifying an effective mass approximation centered around the  $K$  and  $K'$  points of the Brillouin zone. The above success of fitting to a hydrogenic model is also explained by the present microscopic approach because the  $n = 3-5$  exciton wave functions are large enough in spatial extent to predominantly probe the asymptotic  $1/r$  form of the potential given in Eq. (2).

Finally, to study the influence of the material thickness, we monitor the spectral position of the  $2s$  resonance for varying thickness of the  $\text{WS}_2$  sample. Individual derivatives of the reflection contrast are plotted in Fig. 4(a) for the monolayer (1L), bilayer (2L), tetralayer (4L), and bulk. The corresponding energies of the  $1s$  and  $2s$  transitions are shown in Fig. 4(b), with higher excited states masked by additional spectral broadening. Unlike for the case of the monolayer, the bulk excitons are accurately treated with an anisotropic 3D hydrogenic Hamiltonian [42]. Using *ab initio* calculated values, we obtain a bulk exciton binding energy of  $0.05 \text{ eV}$  (see the Supplemental Material [24]), implying a band gap of  $E_g = 2.10 \text{ eV}$ , both of which are in agreement with literature results for bulk  $\text{WS}_2$  [43]. As the layer thickness decreases, the  $2s$  resonance shifts to higher energies, while the  $1s$  resonance remains relatively unchanged, implying a strong increase in both the exciton binding energy and the quasiparticle band gap. Both shifts are found to be large in absolute energies but opposite in sign. This explains the small change in the transition energy of the exciton ground state,

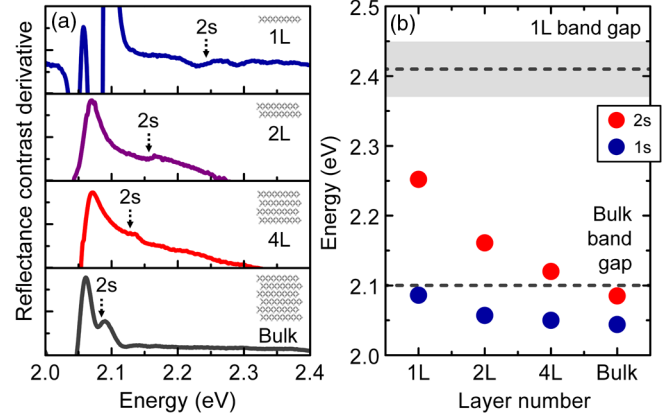


FIG. 4 (color online). (a) The derivative of the reflectance contrast spectra for the  $\text{WS}_2$  1L, 2L, 4L, and bulk. The positions of the  $2s$  exciton resonance are indicated by dotted arrows. (b) Energies of the  $1s$  and  $2s$  states for various layer thicknesses. Band gaps of the bulk and the monolayer are represented by the dashed lines.

similar to findings reported for quasi-one-dimensional systems [39].

The large binding energy of  $0.32 \text{ eV}$  and the non-hydrogenic behavior of the intraexcitonic states in monolayer  $\text{WS}_2$  are expected to be features common to other monolayer TMD materials, based on the strong similarity of their electronic structure. Even larger values of the binding energy are expected for suspended and undoped layers, although the system investigated here corresponds to the typical experimental scenario. Such large binding energies imply high thermal stability of the excitons in comparison to more conventional semiconductors, resulting in a purely excitonic character of emission and absorption at room temperature. Combined with the strong light-matter interaction, this renders atomically thin TMD materials suitable for potential applications in optoelectronic and photonic devices in the visible spectral range. The increased strength of Coulomb interactions at larger distances highlighted in this work suggests that higher-order excitonic effects, such as trion and biexciton formation, are likely to be particularly significant. More generally, the presence of strong and distinctive Coulomb interactions opens up possibilities for fundamental studies of the many-body physics in 2D materials, as well as for novel device applications.

This work was supported in part by the Center for Redefining Photovoltaic Efficiency through Molecule Scale Control, an Energy Frontier Research Center funded by the U.S. Department of Energy, Office of Science, Office of Basic Energy Sciences, under Award No. DE-SC0001085. Support for the reflection contrast measurements was also provided by the National Science Foundation through Grants No. DMR-1122594 and No. DMR-1124894. A. C. gratefully acknowledges funding from the Alexander von Humboldt Foundation within the Feodor-Lynen Fellowship

Program. T.C.B. was supported in part by the U.S. Department of Energy, Office of Science, under Contract No. DE-AC05-06OR23100. H.M.H. and A.R. were supported by the NSF through an IGERT Fellowship (Grant No. DGE-1069240) and through a Graduate Research Fellowship, respectively. This work was carried out in part at the Center for Functional Nanomaterials, Brookhaven National Laboratory, which is supported by the U.S. Department of Energy, Office of Basic Energy Sciences, under Contract No. DE-AC02-98CH10886 (M. S. H.).

*Note added.*—After submission of our paper, several additional experimental and theoretical reports on the excitonic properties of monolayer TMDs have appeared [44].

\*aac2183@columbia.edu

†tony.heinz@columbia.edu

- [1] K. S. Novoselov, D. Jiang, F. Schedin, T. J. Booth, V. V. Khotkevich, S. V. Morozov, and A. K. Geim, *Proc. Natl. Acad. Sci. U.S.A.* **102**, 10451 (2005).
- [2] K. F. Mak, C. Lee, J. Hone, J. Shan, and T. F. Heinz, *Phys. Rev. Lett.* **105**, 136805 (2010).
- [3] T. Li and G. Galli, *J. Phys. Chem. C* **111**, 16192 (2007).
- [4] A. Splendiani, L. Sun, Y. Zhang, T. Li, J. Kim, C.-Y. Chim, G. Galli, and F. Wang, *Nano Lett.* **10**, 1271 (2010).
- [5] L. Britnell, R. M. Ribeiro, A. Eckmann, R. Jalil, B. D. Belle, A. Mishchenko, Y.-J. Kim, R. V. Gorbachev, T. Georgiou, S. V. Morozov, A. N. Grigorenko, A. K. Geim, C. Casiraghi, A. H. Castro Neto, and K. S. Novoselov, *Science* **340**, 1311 (2013).
- [6] J. S. Ross, S. Wu, H. Yu, N. J. Ghimire, A. M. Jones, G. Aivazian, J. Yan, D. G. Mandrus, D. Xiao, W. Yao, and X. Xu, *Nat. Commun.* **4**, 1474 (2013).
- [7] W. Zhao, Z. Ghorannevis, L. Chu, M. Toh, C. Kloc, P.-H. Tan, and G. Eda, *ACS Nano* **7**, 791 (2013).
- [8] K. F. Mak, K. He, J. Shan, and T. F. Heinz, *Nat. Nanotechnol.* **7**, 494 (2012).
- [9] H. Zeng, J. Dai, W. Yao, D. Xiao, and X. Cui, *Nat. Nanotechnol.* **7**, 490 (2012).
- [10] T. Cao, G. Wang, W. Han, H. Ye, C. Zhu, J. Shi, Q. Niu, P. Tan, E. Wang, B. Liu, and J. Feng, *Nat. Commun.* **3**, 887 (2012).
- [11] A. M. Jones, H. Yu, N. J. Ghimire, S. Wu, G. Aivazian, J. S. Ross, B. Zhao, J. Yan, D. G. Mandrus, D. Xiao, W. Yao, and X. Xu, *Nat. Nanotechnol.* **8**, 634 (2013).
- [12] K. F. Mak, K. He, C. Lee, G. H. Lee, J. Hone, T. F. Heinz, and J. Shan, *Nat. Mater.* **12**, 207 (2012).
- [13] D. Lembke and A. Kis, *ACS Nano* **6**, 10070 (2012).
- [14] H. Haug and S. W. Koch, *Quantum Theory of the Optical and Electronic Properties of Semiconductors*, 5th ed. (World Scientific, Singapore, 2009).
- [15] A. Ramasubramaniam, *Phys. Rev. B* **86**, 115409 (2012).
- [16] H.-P. Komsa and A. V. Krasheninnikov, *Phys. Rev. B* **86**, 241201(R) (2012).
- [17] H. Shi, H. Pan, Y.-W. Zhang, and B. I. Yakobson, *Phys. Rev. B* **87**, 155304 (2013).
- [18] D. Y. Qiu, F. H. da Jornada, and S. G. Louie, *Phys. Rev. Lett.* **111**, 216805 (2013).
- [19] G. Berghäuser and E. Malic, *Phys. Rev. B* **89**, 125309 (2014).
- [20] C. Klingshirn, *Semiconductor Optics*, 2nd ed. (Springer, Berlin, 2007).
- [21] L. V. Keldysh, *JETP Lett.* **29**, 658 (1979).
- [22] P. Cudazzo, I. V. Tokatly, and A. Rubio, *Phys. Rev. B* **84**, 085406 (2011).
- [23] T. C. Berkelbach, M. S. Hybertsen, and D. R. Reichman, *Phys. Rev. B* **88**, 045318 (2013).
- [24] See Supplemental Material at <http://link.aps.org/supplemental/10.1103/PhysRevLett.113.076802>, which includes Refs. [25–37], for additional details on sample characterization, optical microscopy, spectroscopy, and theoretical and computational methodology.
- [25] P. Tonndorf, R. Schmidt, P. Böttger, X. Zhang, J. Börner, A. Liebig, M. Albrecht, C. Kloc, O. Gordan, D. R. T. Zahn, S. Michaelis de Vasconcellos, and R. Bratschitsch, *Opt. Express* **21**, 4908 (2013).
- [26] J. Wilson and A. Yoffe, *Adv. Phys.* **18**, 193 (1969).
- [27] H. R. Gutiérrez, N. Perea-López, A. L. Elías, A. Berkdemir, B. Wang, R. Lv, F. López-Urías, V. H. Crespi, H. Terrones, and M. Terrones, *Nano Lett.* **13**, 3447 (2013).
- [28] W. Zhao, Z. Ghorannevis, A. K. Kumar, J. R. Pang, M. Toh, X. Zhang, C. Kloc, P. H. Tan, and G. Eda, *Nanoscale* **5**, 9677 (2013).
- [29] C. Lee, H. Yan, L. E. Brus, T. F. Heinz, J. Hone, and S. Ryu, *ACS Nano* **4**, 2695 (2010).
- [30] E. Hecht, *Optics*, 4th ed. (Addison-Wesley, Reading, MA, 2001).
- [31] S. Byrnes, Multilayer Thin Film Optics Calculator, <http://sjbyrnes.com/>.
- [32] I. H. Malitson, *J. Opt. Soc. Am.* **55**, 1205 (1965).
- [33] *Handbook of Optics*, 3rd ed., edited by M. Bass, C. DeCusatis, J. Enoch, V. Lakshminarayanan, G. Li, C. MacDonald, V. Mahajan, and E. V. Stryland (McGraw-Hill, New York, 2009), Vol. IV.
- [34] C. Zhang, H. Wang, W. Chan, C. Manolatu, and F. Rana, *Phys. Rev. B* **89**, 205436 (2014).
- [35] P. Giannozzi *et al.*, *J. Phys. Condens. Matter* **21**, 395502 (2009).
- [36] J. Deslippe, G. Samsonidze, D. A. Strubbe, M. Jain, M. L. Cohen, and S. G. Louie, *Comput. Phys. Commun.* **183**, 1269 (2012).
- [37] J. P. Perdew, K. Burke, and M. Ernzerhof, *Phys. Rev. Lett.* **77**, 3865 (1996).
- [38] E. Hanamura, N. Nagaosa, M. Kmagai, and T. Takagahara, *Mater. Sci. Eng. B* **1**, 255 (1988).
- [39] J. Deslippe, M. Dipoppa, D. Prendergast, M. V. O. Moutinho, R. B. Capaz, and S. G. Louie, *Nano Lett.* **9**, 1330 (2009).
- [40] K. Tanaka, T. Takahashi, T. Kondo, T. Umebayashi, K. Asai, and K. Ema, *Phys. Rev. B* **71**, 045312 (2005).
- [41] D. Xiao, G.-B. Liu, W. Feng, X. Xu, and W. Yao, *Phys. Rev. Lett.* **108**, 196802 (2012).
- [42] A. Baldereschi and M. G. Diaz, *Nuovo Cimento B* **68**, 217 (1970).
- [43] A. R. Beal and W. Y. Liang, *J. Phys. C* **9**, 2459 (1976).
- [44] B. Zhu *et al.*, [arXiv:1403.5108](https://arxiv.org/abs/1403.5108); Z. Ye *et al.*, [arXiv:1403.5568](https://arxiv.org/abs/1403.5568); G. Wang *et al.*, [arXiv:1404.0056](https://arxiv.org/abs/1404.0056); M. M. Ugeda *et al.*, [arXiv:1404.2331](https://arxiv.org/abs/1404.2331); T. Stroucken and S. W. Koch, [arXiv:1404.4238](https://arxiv.org/abs/1404.4238); K. He, N. Kumar, L. Zhao, Z. Wang, K. Fai Mak, H. Zhao, and J. Shan, *Phys. Rev. Lett.* **113**, 026803 (2014).